Genome Biology

RESEARCH

Open Access

Gut microbiota contributes to high-altitude hypoxia acclimatization of human populations

Qian Su[1,5†], Dao-Hua Zhuang[2†], Yu-Chun Li[1†], Yu Chen[3†], Xia-Yan Wang[1†], Ming-Xia Ge[1], Ting-Yue Xue[1], Qi-Yuan Zhang[1], Xin-Yuan Liu[3], Fan-Qian Yin[1], Yi-Ming Han[1], Zong-Liang Gao[1], Long Zhao[1], Yong-Xuan Li[1], Meng-Jiao Lv[1], Li-Qin Yang[1], Tian-Rui Xia[1], Yong-Jun Luo[3*], Zhigang Zhang[2*] and Qing-Peng Kong[1,4*]

†Qian Su, Dao-Hua Zhuang, Yu-Chun Li, Yu Chen, and Xia-Yan Wang contributed equally to this work.

*Correspondence: luo.yongjun@qq.com; zhangzhigang@ynu.edu.cn; kongqp@mail.kiz.ac.cn

[1] Key Laboratory of Genetic Evolution & Animal Models (Chinese Academy of Sciences), Key Laboratory of Healthy Aging Research of Yunnan Province, Kunming Key Laboratory of Healthy Aging Study, KIZ/CUHK Joint Laboratory of Bioresources and Molecular Research in Common Diseases, Kunming Institute of Zoology, Chinese Academy of Sciences, Kunming, Yunnan 650201, China
[2] State Key Laboratory for Conservation and Utilization of Bio-Resources in Yunnan, School of Life Sciences, Yunnan University, Kunming, Yunnan 650091, China
[3] Department of Military Medical Geography, Army Health Service Training Base, Third Military Medical University, Chongqing 400038, China
[4] CAS Center for Excellence in Animal Evolution and Genetics, Chinese Academy of Sciences, Kunming 650223, China
[5] University of Chinese Academy of Sciences, Beijing 100049, China

Abstract

Background: The relationship between human gut microbiota and high-altitude hypoxia acclimatization remains highly controversial. This stems primarily from uncertainties regarding both the potential temporal changes in the microbiota under such conditions and the existence of any dominant or core bacteria that may assist in host acclimatization.

Results: To address these issues, and to control for variables commonly present in previous studies which significantly impact the results obtained, namely genetic background, ethnicity, lifestyle, and diet, we conducted a 108-day longitudinal study on the same cohort comprising 45 healthy Han adults who traveled from lowland Chongqing, 243 masl, to high-altitude plateau Lhasa, Xizang, 3658 masl, and back. Using shotgun metagenomic profiling, we study temporal changes in gut microbiota composition at different timepoints. The results show a significant reduction in the species and functional diversity of the gut microbiota, along with a marked increase in functional redundancy. These changes are primarily driven by the overgrowth of *Blautia A*, a genus that is also abundant in six independent Han cohorts with long-term duration in lower hypoxia environment in Shigatse, Xizang, at 4700 masl. Further animal experiments indicate that *Blautia A*-fed mice exhibit enhanced intestinal health and a better acclimatization phenotype to sustained hypoxic stress.

Conclusions: Our study underscores the importance of *Blautia A* species in the gut microbiota's rapid response to high-altitude hypoxia and its potential role in maintaining intestinal health and aiding host adaptation to extreme environments, likely via anti-inflammation and intestinal barrier protection.

Keywords: Hypoxia exposure, Time-series, *Blautia A*, Intestinal health, Phenotype acclimatization

Background

Gut microbiota, known as the "second human genome", plays an important role in promoting host adaptation to high-altitude hypoxia environment [1, 2]. Compared to Han Chinese individuals living in lowland areas, high-altitude residents exhibit unique species diversity and community composition (e.g., more abundant phylum Firmicutes [3–5] and genus *Prevotella* [6]) which endure adaptive capacity in high-altitude regions [7]. However, our understanding on the contribution of the bacteria in human high-altitude hypoxia acclimatization remains highly controversial. For instance, while a previous study reported similar alpha diversity in the gut microbiota of Tibetans and Han Chinese living on the Qinghai–Tibet Plateau (QTP) [5], a recent investigation found significantly higher alpha diversity in Tibetans than in Han Chinese from the same town on the QTP [8]. Inconsistencies also exist regarding dominant intestinal bacteria in Tibetans, with one study reporting an abundance of *Acinetobacter*, *Pseudomonas*, and *Sphingobacterium* [9], while another study reported enrichment in *Prevotella*, *Faecalibacterium* and *Blautia* [6].

As gut microbial composition can be easily influenced by multiple factors, such as genetic background, ethnicity, lifestyle, diet, and environment [10–12], these conflicting observations in gut microbiota dynamics in humans exposed to high altitudes could be attributable to factors such as host genetic background or population stratification. Therefore, longitudinal studies of the gut microbiota within the same cohort would be indispensable to reconstruct the temporal dynamics of intestinal changes (composition and function) during high-altitude exposure, thereby facilitating the identification of potential core microbiota that may contribute to host adaptation to hypoxia extreme environments.

In the current study, we conducted a time-series metagenomic investigation of the gut microbiota in a cohort of 45 adult males (Han Chinese) from the lowland plains (243 masl) who moved to the QTP (3658 masl) for 73 days, after which 20 participants returned to the lowland areas. We also obtained the gut metagenomic data of 163 additional adult males (Han Chinese) living in Shigatse, Xizang (4700 masl), with different duration times (from 5 to 60 months) as an independent validation cohort. Based on whole-genome shotgun metagenomic sequencing of fecal samples collected at (1) short-term: one cohort in seven timepoints and (2) long-term: different populations in six timepoints, we investigated dynamic changes in gut microbiota at different stages of high-altitude exposure. The results indicated that short-term hypoxia significantly altered the gut microbiota composition, especially in the early exposure stage. This change was primarily modulated by the increased abundance of *Blautia A* species, which was also prevalent in Han Chinese and Tibetan cohorts acclimatized to high altitudes for 5–60 months. Animal experiments confirmed the role of *Blautia A* in facilitating host fitness to hypoxia environments, likely via anti-inflammation and intestinal barrier protection to maintain intestinal health. Overall, the study underscores the rapid adaptability of human gut microbiota to hypoxic stress and the pivotal role of core bacteria (e.g., *Blautia A* species) in enhancing hypoxic adaptability and maintaining gut health, laying the groundwork for gut microbiota-based interventions in hypoxia-related disorders.

Results

Study overview

Forty-five adult male participants were recruited in this study (age 24.3 ± 1.75 years (mean ± standard deviation (SD)), body mass index (BMI) of 22.17 ± 1.94 kg/m^2). In total, 256 fecal samples were collected from the cohort at 7 timepoints and whole-genome shotgun metagenomic sequencing (WGSMS) of each sample was performed (Fig. 1A). We generated 3.35 Tb of high-quality sequencing data (average 13.4 Gb per sample) (Additional file 2: Table S1). According to the 95% average nucleotide identity (ANI) threshold [13], a non-redundant genome set consisting of 4312 species-level genome bins (SGBs) was constructed based on these data and a previously published human microbial genome [14]. Finally, 1079 SGBs (considered as the presence of each SGB per sample if at least 40% genome coverage was found) were used for subsequent analyses (Additional file 1: Figure S1; Additional file 2: Table S2) [15].

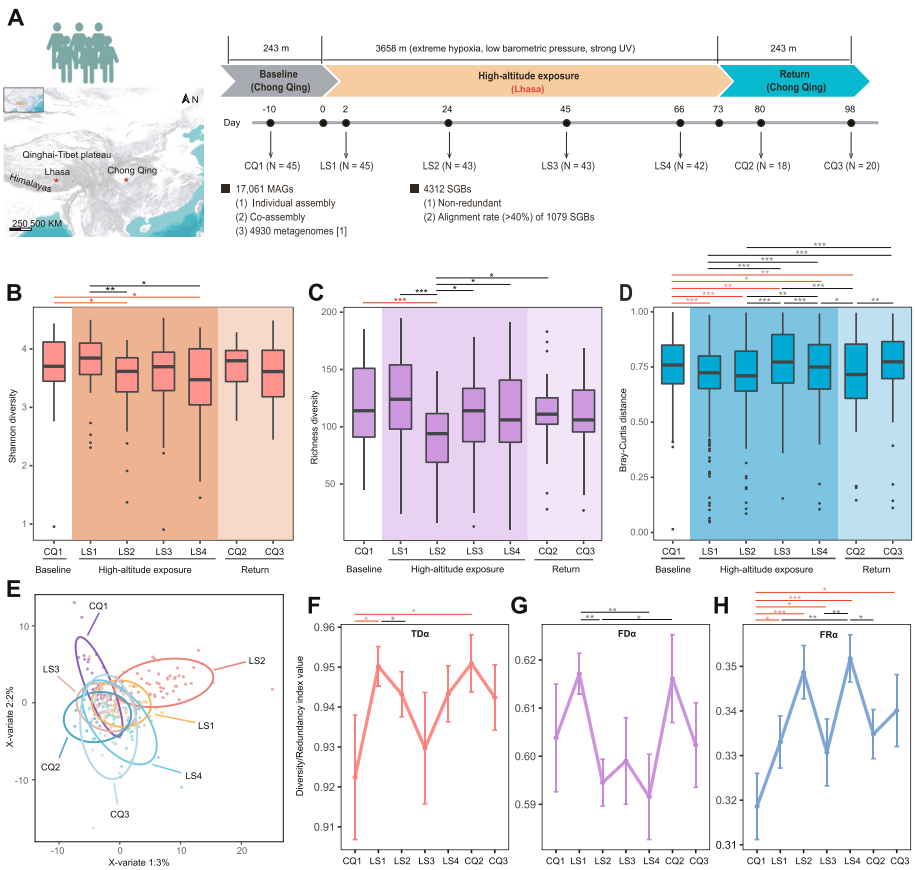

Fig. 1 Overview of high-altitude hypoxia exposure cohort and gut microbiota diversity characteristics. **A** Overview of study design, including longitudinal analysis of human fecal samples at seven timepoints. **B–C** Alpha diversity (Shannon and richness indices) of gut microbiota shows dynamic changes. **D** Intragroup Bray–Curtis distance at different timepoints. **E** Partial least squares discriminant analysis (*PLS-DA*) reveals significant differences in microbial community at different timepoints. **F–H** Alpha taxonomic diversity (TDα, via the Gini–Simpson index), alpha functional diversity (FDα, via Rao's quadratic entropy), and alpha functional redundancy (FRα, as TDα minus FDα) were quantified at each timepoint using 1079 SGBs. For **B–D** and **F–H**, data represent the mean ± SE. Differences between specific timepoints and baseline are indicated with red lines. *$P < 0.05$, **$P < 0.01$, ***$P < 0.001$ by Wilcoxon rank sum test

In addition, we supplemented 163 WGSMS data from 6 cohorts of Han Chinese who lived in Shigatse, Xizang (4700 masl), for ~ 5–60 months. The age (23 ± 3.11 years (mean ± SD)) and BMI index (21.71 ± 2.071) of these participants were similar to those of the short-term time-series cohort (Additional file 2: Table S3). Using the same analysis strategy, we obtained a total of 4262 SGBs. Finally, 1166 SGBs with genome coverage greater than 40% were retained for abundance calculation and analyses at the phylum and genus levels (Additional file 1: Figure S2; Additional file 2: Table S4).

Gut microbiota diversity varied temporally with high-altitude hypoxia exposure

To investigate whether gut microbial diversity varies temporally during exposure, we analyzed alpha diversity (Shannon and richness indices) (Fig. 1B and C; Additional file 2: Table S5) of the gut microbiota over time. To exclude the influence of low-prevalence SGBs, only SGBs in at least 10% of samples were included [16]. Compared with baseline, gut microbial diversity showed non-significant changes within the first 2 days of exposure (LS1; $P > 0.05$). Afterwards, a significant decrease in the Shannon and richness indices was observed in the LS2 stage ($P < 0.05$). In the later stages (exposed for 45 and 66 days, defined as LS3 and LS4, respectively), the richness index recovered, while the Shannon index remained lower than baseline at the end of exposure (LS4; $P < 0.05$), indicating that the rapid decline in bacterial species occurred primarily during the initial period of exposure. Although late adaptation to the plateau was accompanied by an increase in low-abundance bacterial species, Shannon diversity index of the entire microbial community did not recover to baseline levels. Interestingly, gut microbial diversity levels increased to baseline when returned to the lowland plains (7 and 25 days after the end of exposure, defined as CQ2 and CQ3, respectively), supporting a close relationship between altitudinal changes and gut microbial diversity.

We also compared beta diversity at different timepoints (Fig. 1D; Additional file 2: Table S6). In the early stages of exposure, intragroup beta diversity distances became significantly decreased ($P_{LS1,\ LS2} < 1e-7$), implying that the microbial community composition among participants was increasingly similar with each other. However, intragroup beta diversity distances increased at the later stages of exposure (LS3 and LS4; $P_{LS4} > 0.05$), suggesting recovery of microbial differences among participants. Furthermore, the community composition also differed significantly ($P = 0.001$, PERMANOVA) across timepoints (Fig. 1E; Additional file 1: Figure S3).

Functional redundancy of intestinal microbial community increased during exposure

To investigate the functional consequences of altered gut microbiota diversity, we assessed functional redundancy in our cohort using genomic content network (GCN) matrix analysis [17] to estimate the role of microbiota diversity in ecosystem function [18]. Alpha taxonomic diversity (TD_α), alpha functional diversity (FD_α), and alpha functional redundancy (FR_α) were calculated at each timepoint (Fig. 1F-H; Additional file 2: Table S7). Despite fluctuations, a general trend of elevated FR_α and TD_α contrasted with diminished FD_α was noted under exposure (LS1–LS4). In the early stages (LS1–LS2), the relative stability of TD_α was disrupted, as reflected by the significant decrease in microbial species and entropy, suggesting that the core status of CQ1-dominant bacteria was weakened. The changes in FD_α showed that the function of the remaining microbiota

tended to converge after LS1, with several gut microorganisms depleted with exposure. Furthermore, principal coordinates analysis (PCoA) also supported a more concentrated functions during exposure (Additional file 1: Figure S4). This functional convergence resulted in an increase in functional redundancy, which greatly reduced functional diversity loss due to the loss of specific bacterial species [19]. With gradual adaptation to high-altitude, TD_{α} and FD_{α} finally reached equilibrium, but FR_{α} remained higher than baseline at the end of the return stages (CQ3; pFDR = 0.04). These results suggest that the gut microbiota exhibits a rapid response to hypoxia exposure, with a marked and persistent increase in FRα. Compared to baseline, the elevated FRα during exposure and its sustained increase upon returning to the plains indicate a robust and enduring driving force of the gut microbiota in healthy adults to maintain community stability under hypoxic conditions [17, 20].

Blautia A abundance increased significantly with high-altitude hypoxia exposure

The observed increase in the functional redundancy of the gut community during continuous high-altitude hypoxia exposure suggests that the microbiota composition might have changed as well. We thus explored the dynamic changes in the community composition of different taxa levels (phylum, genus, and indicator species) (Fig. 2A-C; Additional file 2: Tables S8 and S9). As shown in the taxonomic annotations of the 1079 SGBs (Additional file 2: Table S2), Firmicutes A became the dominant phylum during the exposure stages, followed by Bacteroidetes, Actinobacteria, Firmicutes, Proteobacteria, and Firmicutes C. Among these phyla, only Firmicutes A demonstrated a significant increase in abundance at the end of the exposure period (LS4; pFDR < 0.05; Additional file 2: Table S10). Similarly, Firmicutes A also displayed the highest abundance in the six different populations of long-term Han residents in Shigatse, Xizang (Additional file 1: Figure S2A).

At the genus level, *Blautia A*, *Faecalibacterium*, and *Prevotella* were the dominant bacteria during the exposure period. Among them, the relative abundance of *Blautia A* showed the greatest increase (Additional file 2: Table S8), from a low level at baseline (median ± SD, 4.80% ± 3.45%) to the highest relative abundance across the whole exposure period (21.1% ± 14.7%) (pFDR = 3.80E − 06; Additional file 2: Table S11). Its abundance was consistent with that of the phylum (Firmicutes A) to which it belongs, indicating that it may be the main contributor to the increase in Firmicutes A abundance. Interestingly, compared to baseline, the relative abundances of Firmicutes A and *Blautia A* both declined after the participants returned to the lowland plains (CQ2; Tables S10 and S11). Specifically, the abundance of *Blautia A* declined rapidly to baseline levels (pFDR = 0.14; Additional file 2: Table S11). In the independent validation cohorts from Shigatse, Xizang, who lived in high-altitude hypoxia environments for a longer time (~ 5–60 months), we also observed that the abundance of *Blautia A* stayed as the highest (Additional file 1: Figure S2B), strongly supporting a close association between Firmicutes A, especially its genus *Blautia A*, and high-altitude hypoxia exposure, e.g., rapid and sustained response.

Indeed, at the species level, the abundance of 13 species from *Blautia A* increased during the early stage of exposure (LS1 and LS2), with the relative abundance of two SGBs (SGB5 and SGB7; Additional file 2: Table S2) remaining significantly higher

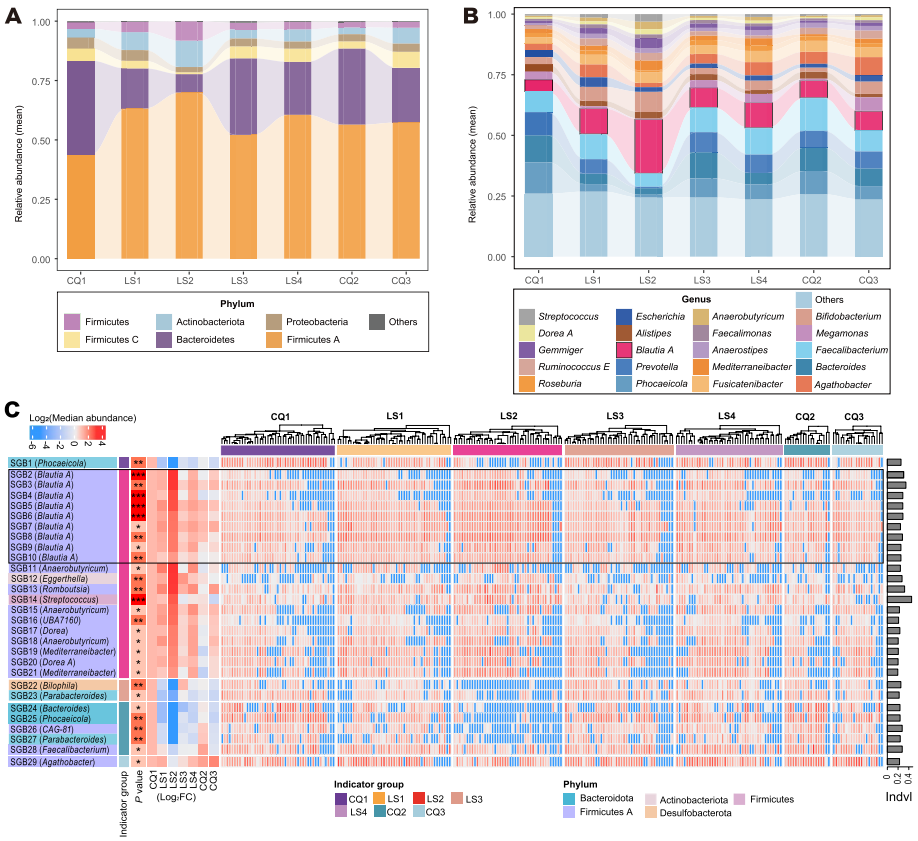

Fig. 2 Time variations in gut microbiota composition of different taxa (phylum, genus, and species). Alluvial plot showing relative abundance dynamics in **A** six most abundant phyla and **B** 20 most abundant genera. Low-abundance taxa are grouped as "others". Ordinate represents mean relative abundance at each timepoint. **C** Heat map showing detailed characteristics of 29 indicator species. Black box highlights details of 9 indicator SGBs from *Blautia A* genus. First column of left panel shows SGB IDs and corresponding genera of 29 indicator SGBs; second column shows group in which the indicator is enriched; third column shows significance of indicator SGBs (*$P < 0.05$, **$P < 0.01$, ***$P < 0.001$); last seven columns show fold changes in median abundance at each timepoint compared to baseline. Baseline group is set to 1. Middle panel shows log10(relative abundance) of each sample at 7 timepoints. "Indvl" in the right panel represents indicator values

than baseline at the end of exposure (LS4; $P < 0.05$; data not shown). Apart from these SGBs, nine additional SGBs exhibited significant increases in relative abundance during the initial stages (LS1-LS2; $P < 0.05$; data not shown) of exposure and sustained the elevations until the culmination at LS4 ($P < 0.05$). Eight of the nine SGBs were members of Lachnospiraceae, e.g., *Anaerostipes hadrus* (SGB130 and SGB131), *Agathobacter rectalis* (SGB29), *Agathobacter sp900546625* (SGB83) and *Blautia A sp000436615* (SGB31). These observations collectively indicated although the abundance of *Blautia A* species started to decline during the later exposure stages (likely due to structural changes of gut microbiota); their roles in response to high-altitude hypoxia exposure sustained until the end of the exposure stage.

Blautia A potentially mediates the decrease of gut microbial diversity

Indicator species are based on the degree of endemicity of bacterial species in different environments and can be used to assess ecosystem health [21, 22]. To determine which core SGBs are potential gut microbial markers associated with high-altitude hypoxia exposure, we performed indicator species analysis (ISA) using SGBs' abundance profile [23]. Altogether, 29 indicator species were distinguished across various timepoints, among which 22 SGBs (SGB2-SGB23) demonstrated discernible responses to the exposure (Fig. 2C; Additional file 1: Figure S5; Additional file 2: Table S9). Among these, 20 SGBs were indicator species of LS2 and 2 SGBs were of LS3 (Additional file 1: Figure S5). Of the 20 indicators in LS2, 9 (9/20, 45%) were from the *Blautia A* genus. The elevated indicator values exhibited by these nine SGBs, coupled with their predominant abundances, strongly indicate that the *Blautia A* genus potentially serves as the pivotal bacteria orchestrating structural alterations within the gut microbiota during high-altitude hypoxia exposure.

Blautia A is extensively involved in multiple functional modules during exposure

To explore the functions corresponding to the changes in community composition reflected by the 29 indicator SGBs, we conducted Kyoto Encyclopedia of Genes and Genomes (KEGG) analysis to predict their functional profiles of module level (Fig. 3; Additional file 2: Table S12). We predicted significantly enriched functional modules at four timepoints (CQ1, LS2, LS3, and CQ2; pFDR < 0.05). Among the enriched pathways of the 20 SGBs (SGB2–SGB21) that were more abundant during the exposure period, the top two were "cofactor and vitamin metabolism" and "energy metabolism", with multiple functional modules concentrated in "cobalamin biosynthesis (map00860: porphyrin metabolism)" and "methanogenesis (map00680: methane metabolism)". Interestingly, these 2 terms remained to be the most enriched functional modules in single-SGB enrichment analysis of the 20 indicator SGBs, with the 9 SGBs from *Blautia A* presenting strong signals (Additional file 1: Figure S6).

To determine how the gut microbiota participates in the "cobalamin biosynthesis" and "methanogenesis" functional modules in response to exposure, we supplemented KEGG ortholog (KO) enrichment of differential SGBs between the baseline (CQ1) and exposure (LS1–LS4) (pFDR < 0.05; Fig. 4). In addition, the self-enrichment of *Blautia A* SGBs was also performed (pFDR < 0.05; Additional file 1: Figure S6). The findings underscored the consistent predominance of these two functional modules throughout the exposure period, concomitant with an escalated abundance of species within the *Blautia A* genus (Fig. 4A and B). In the "cobalamin biosynthesis" module, L-glutamate participates in porphyrin metabolism by multi-step reactions to produce adenosylcobalamin (vitamin B12 coenzyme) (Fig. 4A). In the "methanogenesis" module, Acetyl-CoA decarbonylase/synthase (ACDS) is closely related to the production of methane and acetyl-CoA and transmitted to pathways related to carbohydrate, energy, and amino acid metabolism (Fig. 4B). Of note, *Blautia A* species, containing most enzymes needed for these reactions, participated extensively in the above two modules during the exposure period.

As butyrate-producing bacteria [24, 25], we further used KEGG Mapper tool (https://www.kegg.jp/kegg/mapper/) to conduct pan-genomic analysis of *Blautia A* genus (based

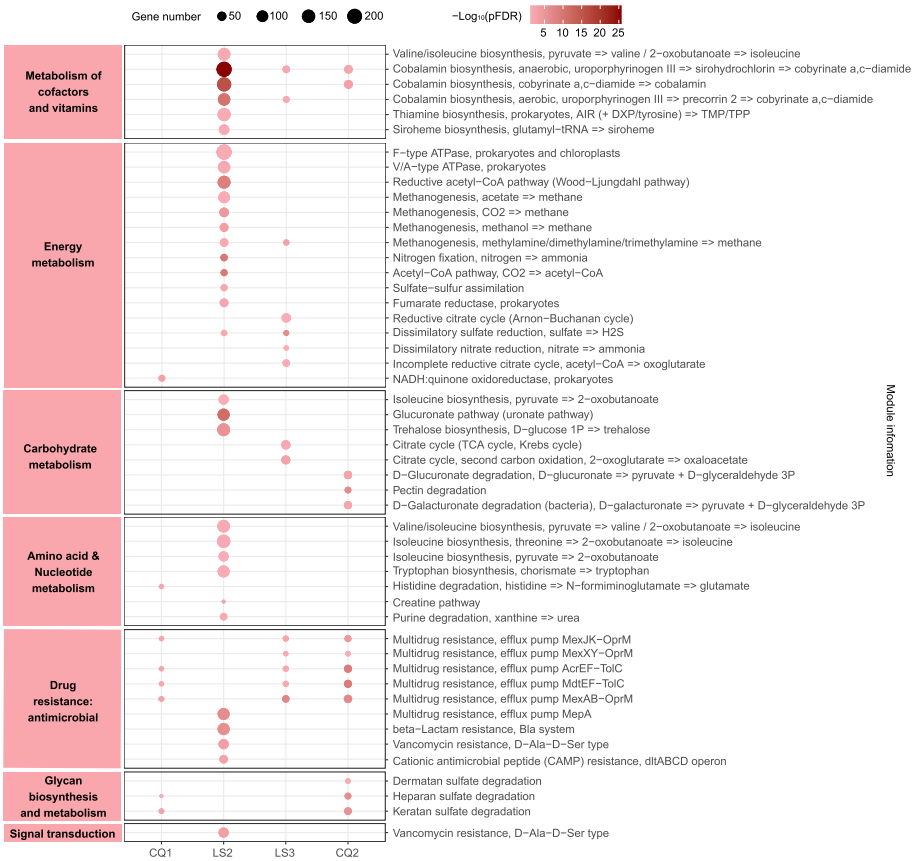

Fig. 3 Dot plot showing enrichment of functional modules of 29 indicator SGBs at different timepoints. LS1, LS4, and CQ3 are not shown since no significant functional modules were enriched at these three timepoints. Left panel corresponds to KEGG metabolism categories. Dot size represents the number of enriched genes in functional modules. Dot color gradient reflects the magnitude of -log10(pFDR) value (Fisher's exact test)

on 12 high-quality SGBs; Additional file 2: Table S2). The results showed that *Blautia A* expressed abundant enzymes of butyric acid production routes, likely via utilizing multiple oligosaccharides through ABC transporters and then synthesizing butyric acid through a series of reactions (Fig. 5). It is worth mentioning that the synthesis capacity of six SGBs (with increased abundance during the exposure) is mainly achieved by regulating pyruvate-related metabolism pathways, which is also reflected in the "methanogenesis" module mentioned above: pyruvate metabolism is enhanced during exposure (Fig. 4B).

Gavage feeding of *B. wexlerae* in mice ameliorated intestinal injury and maladaptation induced by prolonged hypoxia

We next tested the potential role of *Blautia A* under hypoxia exposure by using a mouse model. We chose *B. wexlerae* as the target species due to the following reasons: (1) among the nine indicator species derived from *Blautia A* genus, *B. wexlerae* had the highest relative abundance throughout the entire exposure period. (2) The dynamics of *B. wexlerae* showed the highest consistency with *Blautia A* genus and Firmicutes A phylum (Fig. 2A and B; Additional file 1: Figure S5). Furthermore, we identified *B. wexlerae* DSM19850 (Bw) as a target strain by strict filtering criteria, as detailed in " Methods".

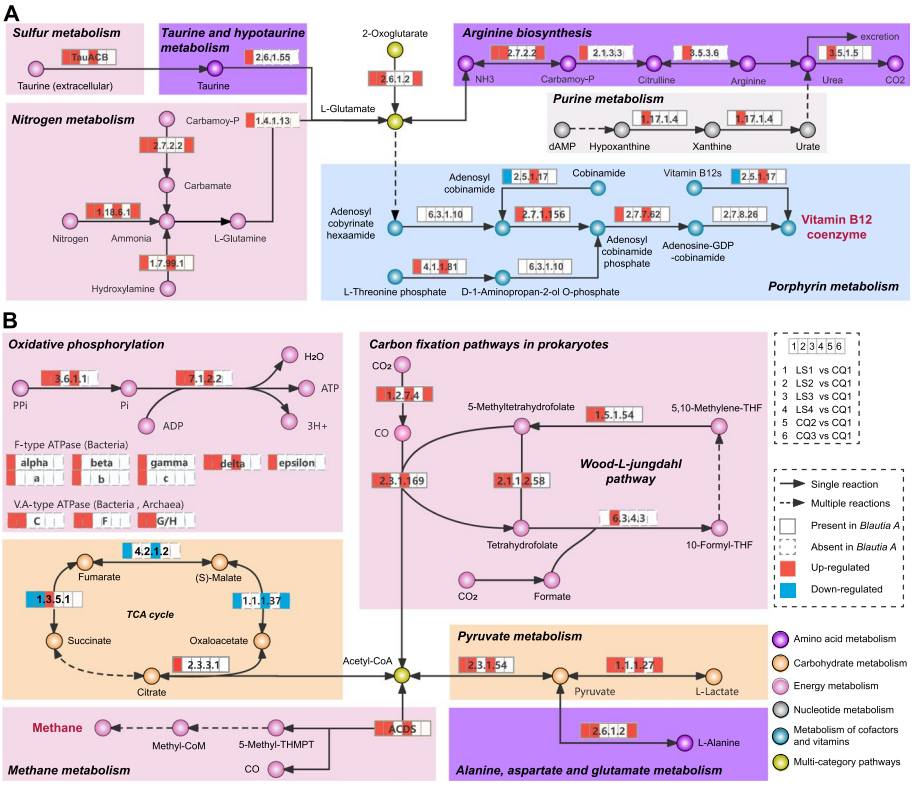

Fig. 4 Dynamics of core functional modules under different high-altitude hypoxia exposure stages based on 1079 SGBs. **A** Reaction steps of cobalamin biosynthesis. **B** Reaction steps of methanogenesis. KOs up-regulated or down-regulated (compared to the baseline) are in red or blue, respectively. KOs enriched in *Blautia A* genome are represented by solid line grid; missing KOs are represented by dotted line grid. The varying colors of the circles represent the classification of metabolites under the KEGG (Level 2) categorization

We conducted a 8-week PBS/Bw gavage supplementation to mice (Fig. 6A). The results showed that the changes in erythrocyte parameters and peripheral oxygen saturation (SpO_2) of HYP + PBS mice were consistent with the aforementioned results from population-based short-term and long-term high-altitude hypoxia exposure surveys, indicating that hypoxia exerted a similar effect on both humans and mice (Fig. 6B; Additional file 1: S7A and S7B). Although there was no significant difference in several hematologic parameters closely related to hypoxia exposure, including hemoglobin (HGB), red blood cell (RBC), mean corpuscular volume (MCV), and hematocrit (HCT), between HYP + Bw and HYP + PBS mice under hypoxia condition (Additional file 1: Figure S7B), significant improvements were observed in SpO_2 (Fig. 6B), pulmonary artery pressure (PAP) in HYP + Bw mice exposed to long-term hypoxia, e.g., significant decreases in right ventricular systolic pressure (RVSP; Fig. 6C) and lung injury score (Fig. 6D), and the decreased deposition of collagen fibers as indicated by less blue staining in lung tissue (pulmonary edema characteristics; Fig. 6E). These indicated an amelioration of the hypoxia-induced symptoms after Bw treatment.

Since hypoxia exposure can also cause intestinal edema [26], we then explored the effects of Bw on the intestinal health under hypoxia exposure. We observed intestinal status changes mainly occurred in the ileum. In detail, HYP + Bw mice

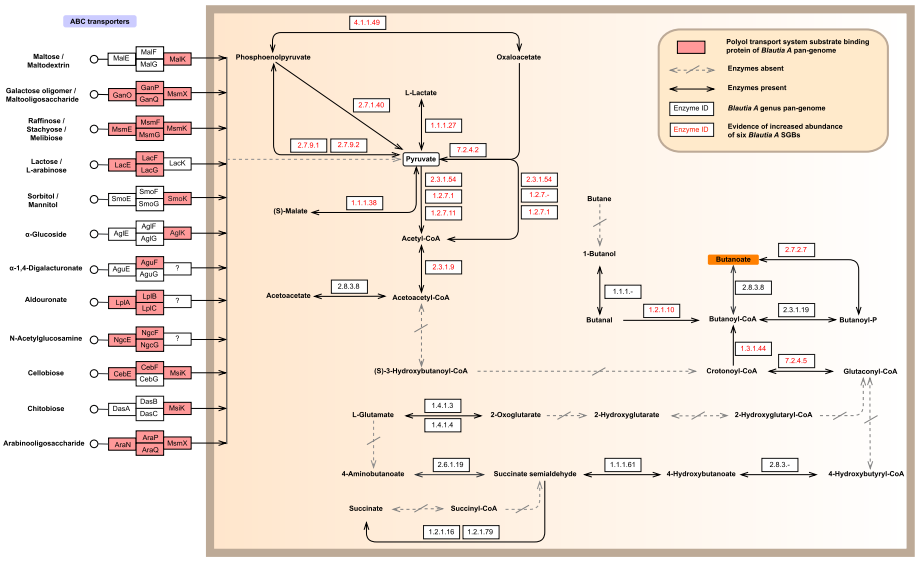

Fig. 5 Butyric acid production routes based on pan-genome analysis of *Blautia A* SGBs**.** Twelve high-quality *Blautia A* SGBs are used for pan-genome analysis. Several pan-genome pathway maps predicted by KEGG database are integrated. Compared with the background 1067 SGBs, the 12 SGBs of *Blautia A* is rich in the "Butanoate metabolism" pathway (pFDR = 0.03). The pink box in the ABC transporter column represents the polyol transport system substrate-binding protein that *Blautia A* can utilize. The orange background box represents the end product

showed a visible improvement of the ileal edema and less gas accumulation than the HYP + PBS mice under hypoxia (Fig. 6F; Additional file 1: Figure S7C). Meanwhile, compared with HYP + PBS mice, HYP + Bw mice exhibited a mild disease process in the ileum, including a significant decrease level of histological injury score (Fig. 6G and H). Pathological sections of the ileum revealed an increasing trend in villus length and crypt depth (Additional file 1: Figure S7D). Accordingly, the expression levels of pro-inflammatory factors IL-1α and IL-1β were elevated in the ileum of HYP + PBS mice compared to NOR + PBS mice, but were significantly suppressed in HYP + Bw mice, suggesting that Bw significantly reduced hypoxia-induced inflammation (Fig. 6I). Intestinal permeability is governed by specific tight junction proteins, with ZO-1 serving as the key marker of tight junction integrity. An increase in intestinal permeability can compromise gut barrier function, leading to potential health issues [27]. Results showed a significant increase in ZO-1 mRNA expression levels ($p = 0.01$) in HYP + Bw mice compared to HYP + PBS mice (Fig. 6J), suggesting that Bw feeding may help restore and maintain the integrity of the intestinal barrier.

Moreover, we analyzed fecal metagenomic data from mice at different sampling timepoints to determine gut microbiota dynamics. The results indicated that the abundance of Bw remains unchanged (Additional file 1: Figure S8A), consistent with previous studies suggesting that gavage supplementation with Bw cannot establish colonization in the gut [28], and there were no significant differences in beta diversity between groups at any sampling timepoints (Additional file 1: Figure S8B). However, under hypoxic exposure, the alpha diversity, particularly the Shannon index and evenness index, significantly decreased in HYP + Bw mice compared to HYP + PBS mice (Additional file 1: Figure S9).

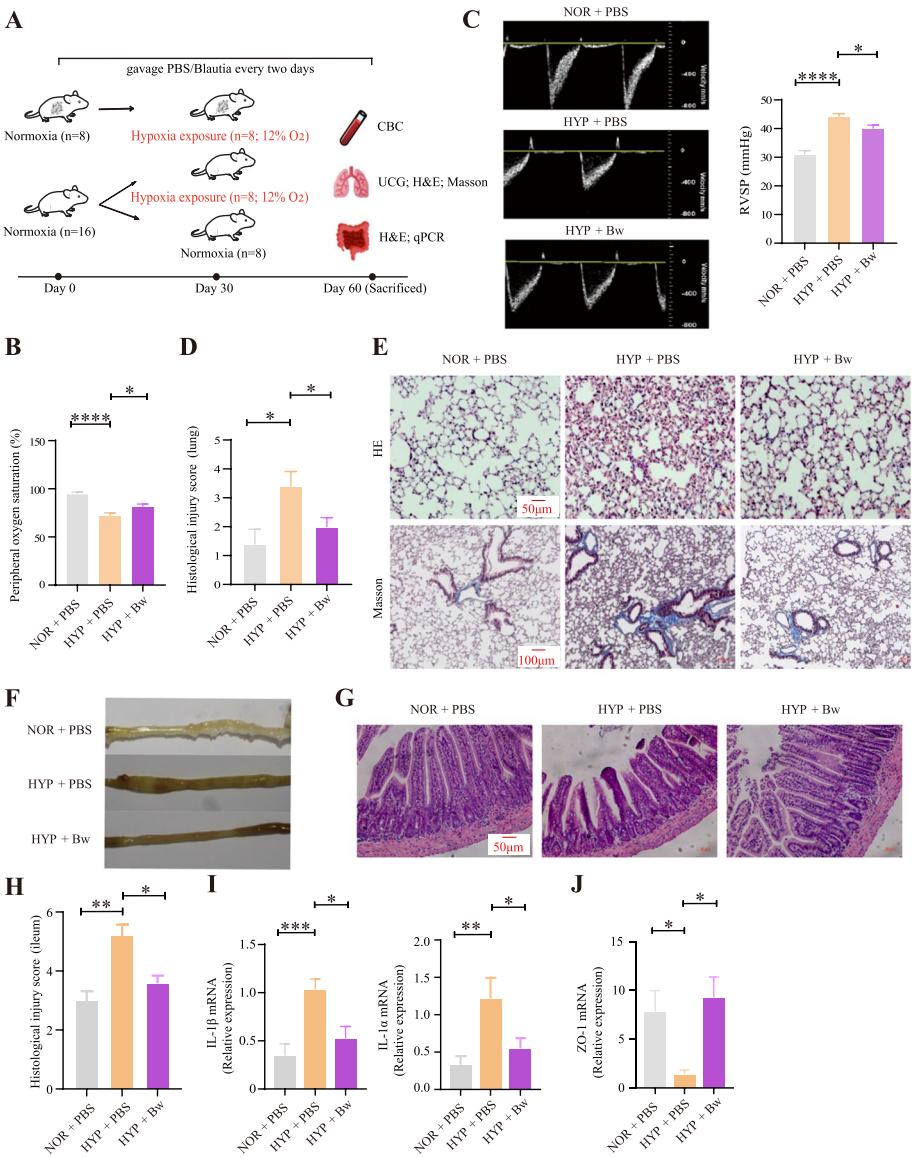

Fig. 6 Gavage feeding of *B. wexlerae* suppresses intestinal inflammation and promotes high-altitude acclimatization.**A** Design of animal experiments. The three groups are as follows: (1) PBS-fed in normoxia for 8 weeks (NOR+PBS); (2) PBS-fed in normoxia for 4 weeks and hypoxia for another 4 weeks (HYP+PBS); (3) *B. wexlerae*-fed in normoxia for 4 weeks and hypoxia for another 4 weeks (HYP+Bw). **B** Peripheral oxygen saturation (SpO_2) of mice ($n = 8$ per group). **C** The quantification of pulmonary artery acceleration time (PAT) is converted by the formula [29] (detailed in "Methods") ($n = 6$–7 per group). **D** Lung histological injury score of mice ($n = 5$ per group). **E** Representative H&E and Masson trichrome-stained of the mice lung sections ($n = 5$ per group). **F** Gross images of the mice distal ileum ($n = 5$ per group). **G** Representative H&E-stained sections of the mice distal ileum ($n = 5$ per group). **H** Statistical analysis of histological injury score of the mice distal ileum ($n = 5$ per group). **I** The relative mRNA expression levels of IL-1α and IL-1β in the ileum ($n = 8$ per group). **J** The relative mRNA expression level of ZO-1 in the ileum ($n = 8$ per group). Data are representative of at least three independent experiments (mean ± SE). $^{*}P < 0.05$; $^{**}P < 0.01$; $^{***}P < 0.001$; ns not significant (one-way ANOVA with Dunnett's multiple comparisons test)

The abundance of Lactobacillaceae (e.g., genus Ligilactobacillus) significantly increased (pFDR < 0.05) and persisted until the last sampling (Additional file 1: Figure S10). These findings highlight that Bw gavage may influence gut microbial diversity and community

composition, thereby alleviating hypoxia-induced gut injury and inflammation and enhancing hypoxia adaptation.

Discussion

Our 108-day longitudinal survey of 45 healthy participants, who were exposed to high altitude (> 3600 masl) for over 2 months, helps to reconstruct the dynamics of gut microbiota under high-altitude exposure and provides a catalog of reference genomes from the human microbiome exposed to hypoxia extreme environments. Our results showed that species and functional diversity of the gut microbiota decreased significantly during the exposure period, suggesting that high-altitude hypoxia exposure has a marked effect on gut microbiota. Interestingly, community composition at the phylum and genus levels changed significantly during exposure, especially in the first month (LS1 and LS2), but recovered upon return to the lowland plains, highlighting the rapid response of gut microbiota to high-altitude hypoxia exposure and the strong regulatory capacity of community homeostasis [7].

Importantly, we determined that the reduction in gut microbiota diversity (indicated by Shannon and richness indices), as well as the marked changes in community composition during high-altitude hypoxia exposure, were largely attributable to the significant increase of *Blautia A* abundance (in both relative (Additional file 2: Table S8) and absolute (Additional file 2: Table S13) abundance). This genus has been reported with high abundance in Han Chinese (who lived on the Tibetan plateau for over 4 years) [5], Tibetans [6], and even wild yak [30], although it has not been identified as the core or the dominant bacterial group in the previous studies, possibly due to the different exposure durations between ours (2–3 months) and the previous studies (over 4 years) or to the distinct research strategies (longitudinal versus cross-sectional). Interestingly, the six additional Han Chinese cohorts living in Shigatse, Xizang (4700 masl), with different durations also exhibited the highest abundance of *Blautia A* (Additional file 1: Figure S2B).

The observation of high *Blautia A* abundance in our short-term and long-term exposed cohorts, as well as the indigenous Tibetans and native animals (i.e., yaks) [30], suggests this genus is most likely the beneficial high-altitude bacterial group that plays an important role in promoting high-altitude acclimatization/adaptation. Indeed, we found that *Blautia A* species widely participated in the "cobalamin biosynthesis" module (Fig. 4A) and butyric acid production (Fig. 5). Cobalamin and butyric acid, with cobalamin being able to promote the production of butyric acid [31], are both beneficial to microbial ecosystems and intestinal epithelial cells and involved in the maintenance of intestinal health and immunomodulation at high-altitude hypoxia environments [32, 33]. In addition, several core species of *Blautia A* (e.g., *B. faecis*), also known to exert anti-inflammatory activities [34], displayed relatively high abundance in our cohort after they were exposed to the high altitude until the end (LS4). Meanwhile, several species of Lachnospiraceae that persist to be higher than the baseline level also have the ability of SCFAs production and anti-inflammation [25, 35], further suggesting that the above functions may be conducive to the high-altitude hypoxia adaptation of the human body.

These findings suggest that *Blautia A* may facilitate adaptation of the gut to high-altitude hypoxia environments by exerting an anti-inflammatory effect. Indeed,

anti-inflammatory function is important for adaptation to extreme environments [36] and intestinal protection of the host. Previous studies indicated that the role of probiotics in the gut mainly presented in the ileum where inflammation and damage occurred during high-altitude hypoxia exposure [37–39]. These anti-inflammatory functions, exerted by *Blautia A*, were further confirmed in our mice experiments, as evidenced by lower levels of intestinal ileal edema, less gas accumulation, and suppressed expression of pro-inflammatory factors in *B. wexlerae* gavage mice. Moreover, *Blautia A* supplementation also can significantly alleviate discomfort symptoms such as decreased SpO_2, pulmonary edema, and increased PAP caused by hypoxia exposure. These results indicate a high potential probiotic role of *Blautia A* under high-altitude hypoxia exposure. However, we also found that *Blautia A* produced methane as a by-product, which can lead to energy loss [40], thus suggesting a side effect of gaining high-altitude acclimatization.

Overall, our study reveals that *Blautia A* may function in anti-inflammation and intestinal barrier protection to maintain intestinal health and enhance host hypoxia adaptability (including significantly improved SpO_2 and lung characteristics). Interestingly, an anti-inflammatory role of the dominant gut microbiota is also the core function in many animals native to the QTP, such as the Tibetan antelope [41], Tibetan pig [9], and Tibetan ass [42], albeit achieved by different microbiota [43]. These observations lend support to the importance of anti-inflammatory functions of gut microbiota in facilitating host adaptation to hypoxia extreme environments such as high altitude, both short-term (acclimatization) and long-term (adaptation).

Conclusions

By conducting a 108-day longitudinal study of the same cohort under high-altitude hypoxia exposure, we studied temporal changes in gut microbiota composition at 7 timepoints using shotgun metagenomic profiling. This study demonstrated how the human gut microbiota rapidly responds to hypoxia stress and identified core gut bacteria (e.g., *Blautia A* species) in response to high-altitude hypoxia exposure. Additionally, the highest abundances of *Blautia A* genus were further validated in additional cohorts living in higher altitude (lower hypoxia) with different duration (~ 5–60 months). In vivo animal experiment supports a crucial role of *Blautia A* species in facilitating host fitness to hypoxia environments, likely via anti-inflammation and intestinal barrier protection to maintain intestinal health, suggesting a high translational potential of *Blautia A* species as a candidate probiotic agent for the prevention or treatment of hypoxia-associated maladaptation or disorders. These results altogether revealed a role of *Blautia A* in facilitating host fitness to hypoxia environments.

Methods

Study design and sample collection

Forty-five male students from Chongqing who went to Lhasa Hospital for health examination were recruited, all of whom traveled from Chongqing to Lhasa by plane on the same day. All of the participants provided informed consent to participant in this study under the approval the Institute Research Medical Ethics Committee of the Army Medical University (Approval number: 2020 No. 011–1) and the Ethics Committee at Kunming Institute of Zoology, Chinese Academy of Sciences (Approval number:

KIZRKX-2021–010). All participants stopped using antibiotics within 30 days or probiotic products within 14 days before the first sample collection (10 days before exposure, treated as baseline). Nine days after the baseline, these participants traveled from Chongqing to Lhasa, Xizang within 1 day. Exclusion criteria for individuals included any history of cardiopulmonary disease, metabolic syndrome, dyslipidemia, and gastrointestinal disease. During the whole sampling process, participants ate in the unit canteen and kept a similar schedule with a unified arrangement of accommodation, which to a large extent eliminated the influence of lifestyle. Finally, 45 participants (BMI, mean ± s.d., 22.23 ± 1.97 kg/m^2) aged 21 to 27 years were included in the study. Fresh fecal samples were collected from subjects in a fasting state in the morning at seven timepoints over a period of 108 days. These included baseline (CQ1), day 2 (LS1), day 24 (LS2), day 45 (LS3), day 66 (LS4), day 80 (CQ2), and day 98 (CQ3) (Fig. 1A). Sampling of 256 samples was completed from July 11 to October 26, 2019, and these samples were transported back to the laboratory using liquid nitrogen on the day of collection, and then stored at − 80°C until further processing. DNA of all samples was extracted together in the sample laboratory within 1 week after the sample collection. Complete blood counts (Sysmex Corporation, Kobe, Japan) and SpO_2 measurements (Yu well, Jiangsu, China) were performed at 7 timepoints for 45 participants.

Metagenomic DNA extraction

Bacterial DNA from fecal samples (200 mg) was extracted using the QIAamp DNA Stool Mini Kit (Qiagen, Germany) according to the manufacturer's instructions. The DNA purity (OD 260/280) was determined using the Nanodrop® spectrophotometer (IMPLEN, CA, USA) and 1% agarose gels, and the DNA concentration was measured using the Qubit® dsDNA Assay Kit in Qubit® 2.0 Fluorometer (Life Technologies, CA, USA). Microbial DNA extraction was performed within 2 months.

Whole-genome shotgun sequencing and data preprocessing

About 2 μg of qualified DNA per sample was used to construct DNA sequencing libraries using the NEBNext® Ultra DNA Library Prep Kit (NEB #E7370L). Libraries were sequenced for 150 bp paired-end model on the Illumina NovaSeq 6000 platform (lllumina, USA). Adapter sequences and low-quality reads in raw data were trimmed using fastp (v0.21.0, options "–trim_poly_g -q 20 -W 4 -M 20 -u 30 -n 5 -y -Y 30 -l 70 -w 10") [44]. Host sequence removal was performed using Bowtie2 (v2.4.4) alignment software [45] and Human Reference Genome (*Hg19*). Finally, 1.61 Tb of high-quality host-free clean data (average 6.31 Gb per sample) was obtained.

Metagenome assembly and contig binning

Host-free clean reads were assemblied by two strategies using MEGAHIT (v1.2.9, option "–min-contig-len 500") [46]: (i) individual assembly (single sample assembly) and (ii) co-assembly (merge sequencing data and assemble them according to each timepoint, respectively). These contigs obtained from both individual assembly and co-assembly were binned using two binning tools, Metabat2 and Maxbin2 integrated in MetaWRAP (v1.2.1) to construct metagenomic-assembled genomes (MAGs) [47].

Notably, we employed co-assembly strategy, which facilitates the retrieval of more genomes in relatively long (> 5) subject-specific time series [14].

The completeness and contamination of MAGs or species-level genomes (SGBs) were assessed using CheckM (v.1.0.12, options "lineage_wf") [48]. Medium-/high-quality MAGs (with completeness greater than 50% and contamination less than 5%) were retained for subsequent analysis; 10,865 and 1266 medium/high MAGs were obtained from individual and co-assembly binning strategies, respectively. In addition, we have integrated a previously published human SGB set [14]. All 12,131 medium/high MAGs and 4930 published SGBs were deduplicated together using dRep (v3.0.0) [49] with 90% primary clustering and 95% secondary clustering ANI, and the highest scoring (using the default scoring calculation formula) MAGs were retained from each secondary cluster as representative genomes. Finally, a total of 4312 SGBs were obtained, 234 of which were from individual assemblies, 37 from co-assemblies, and 4041 from a previous study [14] (Additional file 2: Table S2). To obtain a more accurate SGB abundance profile, 1079 SGBs with genome coverage greater than 40% were reserved for subsequent analysis [15].

Microbial taxonomy, function redundancy analysis, KEGG functional enrichment, and prediction

Taxonomy was assigned to 4312 SGBs using GTDB-tk 1.5.0 [50] and the GTDB (Genome Taxonomy Database) release 207, and a taxonomy dendrogram (Additional file 1: Figure S11) was constructed using GraPhlAn (v1.1.3) [51].

Functional redundancy refers to the portion of alpha taxonomic diversity (TDα) that cannot be explained by alpha functional diversity (FDα) [17]. This concept is crucial for investigating the stability of gut microbiota under high-altitude stress conditions. The calculation method of weighted jaccard similarity matrix is referred to the website https://rpubs.com/lgadar/weighted-jaccard. Then, the matrix is used to calculate the functional redundancy indices. For each group, the Gini–Simpson index was used to characterize the alpha taxonomic diversity (TD_α), and the Rao's quadratic entropy was used to characterize alpha functional diversity (FD_α). The calculation of alpha functional redundancy (FR_α) was as follows [17]:

$$FR_a = \sum_{i=1}^{N} \sum_{j \neq i}^{N} (1 - d_{ij}) p_i p_j$$

All genes from 1079 SGBs were aligned to the KEGG database using DIAMOND (v2.0.9.147, options "blastp –outfmt 6 –sensitive –evalue 1e-5 –id 30"), and the gene with the best hit score was retained [52]. Functional profile was constructed based on the number of genes annotated to each KEGG ortholog (KO) in each sample. Fisher's exact test was used for enrichment analysis (both module level and KO level) (Fig. 3).

We used KEGG Mapper tool (https://www.kegg.jp/kegg/mapper/) to analyze the pan-genome map of "Butanoate metabolism" pathway based on 12 high-quality SGBs of *Blautia A* genus (Additional file 2: Table S2) and explore its butyric acid production route.

Validation populations for long-term residence at high-altitudes

To validate the *Blautia A* signal discovered based on short-term time-series cohort, we supplemented 163 WGSMS data in 6 independent cohorts of Han Chinese who lived in Shigatse, Xizang (4700 masl), for different durations, i.e., 6 ± 1 month, 11 ± 1 month, 18 ± 1 month, 25 ± 1 month, 30 ± 1 month, and ≥ 60 months. Sampling of 163 samples was completed from 20 May to 15 June, 2022. Their age and BMI index were similar to those of the time-series cohort (Additional file 2: Table S3). The sample collection and processing methods were consistent with the time-series cohort. The analysis strategy adopted for metagenomics kept the same with that described above. A total of 7221 medium/high MAGs were obtained from individually binning strategies. After deduplicated, a total of 4262 SGBs were obtained, of which 303 were individually assembled and 3943 were from previous study [14] (Additional file 2: Table S4). At last, 1166 SGBs with genome coverage greater than 40% were reserved for further analysis [15, 53].

Bacterial strain selection and culturation

We selected 13 SGBs of *Blautia A* with significantly increased abundance during the exposure period and downloaded the complete genome sequences of 20 *Blautia A* members recorded by NCBI. Filter criteria for strains include (1) SGB with a similarity of $\geq 95\%$ with 20 *Blautia A* genomes from NCBI ($n = 6$). (2) Above 33 sequences were deduplicated at the strain taxa (–S_ani 0.99) using dRep (v3.0.0) [49], and 10 SGBs were identified, followed by species annotation using GTDB-tk 1.5.0 [50]. Finally, we selected *B. wexlerae*, a species that met the filtering criteria (1) and (2), and the type DSM19850 was used for our subsequent mice experiments. The detailed information were shown in Additional file 2: Table S14.

B. wexlerae (DSM19850) and peptone-yeast-glucose modified broth (PYGm) were purchased from Mingzhoubio (Ningbo, China). As an anaerobic strain, *B. wexlerae* was cultivated in PYGm in an anaerobic chamber (Bactron EZ-2, Shellab, USA) at 37℃ for 48 h. DSMZ protocol was followed during PYGm medium preparation [54]. Cultures were stored as 0.2-ml aliquots in an anaerobic air pouch (Mitsubishi Gas Chemical, Tokyo, Japan) at 4℃ until use for gavage feeding into mice.

The peripheral oxygen saturation measurement

At the end of the seventh week, the mice were stabilized using a collar clamp for at least 20 min, and then the peripheral oxygen saturation (SpO_2) was measured using a ring neck oximetry (MP160, Biopac Systems, Goleta, CA, USA) in the cabin. Each mouse was measured for four times and the average value was taken.

Chocardiography measurement

At the end of the 8th week, all of the 24 mice were anesthetized with sevoflurane and their body weight was recorded. Subsequently, the pulmonary artery acceleration time (PAT) was measured by ultrasonic cardiogram (UCG) and right ventricular systolic pressure (RVSP) was quantified using the formula $y = -1.5x + 63.7$ [55], where RVSP is the gold standard for diagnosing pulmonary artery pressure (PAP). In

detail, hair removal cream was used to remove hair from the chest of mice, and then a high-resolution small animal ultrasound imaging system (Vevo 3100 Fujifilm, Visual Sonics) was used to detect PAT. All steps comply with the requirements of ultrasonic criteria [56]. All measured values were averaged over three cardiac cycles.

Blood and tissue analysis

After euthanizing the mice, complete blood count (CBC) of mice were measured using a hematological analyzer (Mindray BC-5000 Vet). The distal (ileum) segments of small intestine were cleaned with cold PBS and fixed with 4% paraformaldehyde overnight, followed by dehydration in an gradient series of ethanol solutions, embedding in paraffin and sectioning into 4 μm for hematoxylin and eosin (H&E) staining. The lung was harvested and fixed overnight in 4% paraformaldehyde at 4℃. Pareffin sections that with 4 μm thickness were stained with H&E staining and Masson's trichrome staining (Baso, Zhuhai, China). Subsequently, the pathological changes of lung tissue were identified and scanned using an inverted fluorescence microscope (Axio Observer 3, Zeiss, Germany). Semi-quantitative assessment of intestinal and pulmonary pathology was performed in a blinded manner. The damage degree of ileum was evaluated [57], and the height of intact villi and crypt depth were measured using ZEN 2.6 (blue edition). Each slice counts at least five randomly selected regions to minimize slice differences.

Lung histological injury scoring was performed using the following system: the absence or presence of cellular biochemistry received 0 and 1 point, respectively. Regarding lymphocyte infiltration, normal or occasional leukocytes, inflammatory cells were found to be widespread or clustered, and abscess lesions received 0, 1, and 2 points, respectively. For alveolar morphology, the alveolar wall morphology was normal, thickening of alveolar walls or slight dilation of alveolar capillaries, fibroplasia of the alveolar wall and severe vasodilation and hyperemia received 0, 1, 2, respectively. For alveolar exudation, there is no exudation in the alveolar, edema or bleeding, serous, and fibrous and the suppurative luminal exudates that spread to the alveoli received 0, 1, 2, 3, respectively. The scores of these parameters were summed to yield a total histological score from 0 to 8.

Reverse transcription and quantitative PCR (RT-qPCR) analysis

Total RNA was extracted using TRIzol reagent (Invitrogen). The cDNA was prepared using a RevertAid First Strand cDNA Synthesis Kit (Thermo Fisher Scientific, US). Real-time PCR was performed using Fast SYBR Green Master Mix (Thermo Fisher), and the primer sequences were listed in Additional file 2: Table S15. Relative expression to GAPDH was calculated using the $\triangle\triangle$Ct method.

Mice and hypoxia exposure experiments

Twenty-four male C57BL/6 mice (8 weeks old) were purchased from Experimental Animal Center, Yunnan University (Yunnan, China). All mice were maintained under specific pathogen-free conditions and acclimatized for 1 week with free access to food and water under 12-h light/dark cycle. These mice were then divided equally into three groups by random selection (eight mice in each group), of which two groups were further fed with PBS and one group with *B. wexlerae*. After 4 weeks of feeding under normal

oxygen, one group of PBS mice continued to receive normoxic gavage for 4 weeks, while the other group of PBS mice and *B. wexlerae* mice were fed under hypoxia conditions for another 4 weeks (12% O_2, equivalent to the oxygen level at ~ 4000 m).

We adopted the experimental protocol of mice gavage following previous studies [28, 58, 59]. In detail, during the whole process of the experiments (totally lasted for 8 weeks), all mice were free to obtain food and water and received 0.2 ml of bacterial solution (1×10 9 CFU/ml) or PBS by gavage every 2 days. The weight of each mouse was calculated weekly. At 8 weeks, mice were euthanized by cervical dislocation, followed by tissue collection using surgical scissors. All animal procedures in our study were conducted in accordance with the guidelines approved by the Ethics Committee of the Kunming Institute of Zoology (Approval number: IACUC-RE-2023–05-010).

Metagenomic sequencing analysis in mice

Fecal samples from mice were collected at seven timepoints: baseline (0 days), 14, and 30 days under normoxia and 3, 7, 11, and 14 days under hypoxia. Increased sampling frequency under hypoxia aimed to better capture the gut microbiota shifts. A total of 126 fecal samples ($n = 6$ per group) were obtained. Consistent with the aforementioned methods, we conducted whole-genome shotgun sequencing using the Illumina NovaSeq 6000 platform (Illumina, USA) at Biolinker Technology Co., Ltd. (Kunming, China) and then performed the data preprocessing. Host sequence removal was performed using Bowtie2 (v2.4.4) alignment software [45] and Mus musculus Reference Genome (*GRCm39*). Using Metaphlan4 software, we generated abundance matrices [60]. The Bw strain genome sequence, downloaded from NCBI, served as the reference for analyzing the colonization dynamics of samples at different intervals. The results showed that all 126 samples met the standard of greater than 40% genome coverage and were subsequently used for the colonization analysis of Bw [15].

Statistical analysis

All statistical analyses were performed with R (v4.1.3) in RStudio platform or python (v2.7.15/v3.8.10) in Linux platform. The alpha diversity (Shannon, richness, and evenness), Bray–Curtis distance, and principal coordinates analysis (PCoA) were investigated using R-package *vegan* (v2.5.7) [29]. The adjusted R^2 in PCoA analysis was performed using the function "*RsquareAdj*". The permutation multiple analysis of variance (PERMANOVA) was calculated the p value using the "*adonis2*" function. Partial least squares discriminant analysis (*PLS-DA*) was performed using R-package *mixOmics* (v6.18.1) [61]. Here, we defined SGBs that exist in at least 50% of 256 samples (core 50) as core species [62], and the indicator species analysis was performed using the function "*indval*" in R-package *labdsv* (v4.1.3) [23] based on the abundance profile of core species.

The significance level between groups of SGBs' abundance and functional redundancy indices ($FR_{\alpha,}$ FD_{α}, and TD_{α}) were determined by Wilcoxon rank sum test (paired), and the rest of the group difference tests were determined using Wilcoxon rank sum test (unpaired). The enrichment analyses were performed by Fisher's exact test. *P* values were adjusted using the false discovery rate (FDR) approach with the function "*p.adjust*".

Data analyses of mice experiments were performed using GraphPad Prism 8 (GraphPad Software Inc., San Diego, CA, USA). For each assay or phenotypic

analysis, data from multiple experiments were averaged (mean ± SD) and evaluated for statistical significance through suitable tests. One-way ANOVA was applied for multiple comparisons, with post-hoc analysis identifying *P* values.

Supplementary Information

The online version contains supplementary material available at https://doi.org/10.1186/s13059-024-03373-w.

Additional file 1: Supplementary Figures S1 to S11.

Additional file 2: Supplementary Tables S1 to S15.

Additional file 3: Review history.

Acknowledgements
We thank Prof. Bing Su and Dr. Yongbo Guo (Kunming Institute of Zoology, Chinese Academy of Sciences) for providing us with polycarbonate hypoxic chamber (Coy Laboratory Products); Mr. Dong Li (School of Life Sciences, Sichuan Agricultural University) for the experiment guidance; and Han Xu and Zhenhua Liu (Kunming Institute of Zoology, Chinese Academy of Sciences) for the helpful discussion and experimental assistance. We also thank Dr. Christine Watts for her help in honing the text.

Peer review information
Kevin Pang and Tim Sands were the primary editors of this article and managed its editorial process and peer review in collaboration with the rest of the editorial team.

Review history
The review history is available as Additional File 3.

Authors' contributions
Q.-P.K. designed the study. Y.-C.L., Y.-J.L., Y.C., M.-X.G., F.-Q.Y., Y.-M.H., Z.-L.G., L.Z., and L.-Q.Y. collected the samples and conducted the experiments. Q.S., D.-H.Z., Z.G.Z., T.-Y.X., and Q.-Y.Z. analyzed the data. X.-Y.W. analyzed experimental data from mice. Y.-X.L. detected mouse transcription levels using RT-qPCR. M.-J.L. fed mice. Q.S. and D.-H.Z. wrote the manuscript. Y.-C.L., Q.-P.K., and Z.G.Z. provided suggestions and modified the manuscript. All authors approved the final version of the manuscript.

Funding
This work was supported by the Second Tibetan Plateau Scientific Expedition and Research (2019QZKK0607; 2019QZKK0503), Yunnan Fundamental Research Projects (No. 202401AS070073), the Major Science and Technology Project in Yunnan Province of China (No. 202001BB050001), CAS "Light of West China" Program (Y.-C.L.), High-level Talent Promotion and Training Project of Kunming (Spring City Plan; 2020SCP001), Yunling Scholar of Yunnan Province (Q.-P.K.; Z.G.Z.), Yunnan Ten Thousand Talents Plan Young & Elite Talents Project (Y.-C.L.), Yunnan Fundamental Research Projects (202201AW070012), National Natural Science Foundation of China (No.U2002206 and 31970571), the central government guides local science and technology development funds (Z.G.Z.), and Hainan Provincial Natural Science Foundation of China (ZDYF2021SHFZ227).

Availability of data and materials
All human metagenomic sequencing data from this study have been deposited in the Genome Sequence Archive [63] in National Genomics Data Center [64], China National Center for Bioinformation/Beijing Institute of Genomics, Chinese Academy of Sciences (GSA: HRA003616) that are publicly accessible at https://ngdc.cncb.ac.cn/gsa-human [65]. The metagenomic sequencing data of hypoxia-exposed mice from this study have been deposited in GSA (CRA018138) that are publicly accessible at https://ngdc.cncb.ac.cn/gsa [66]. The reference information for public dataset [67] and genomes used in this study is summarized in Tables S2 and S4. The images from lung and ileal histological sections in this work have been made freely available (https://zenodo.org/records/13147420) [68]. All mouse and human data generated in this study, as well as any other information related to this research, can be obtained from the corresponding author (Dr. Qing-Peng Kong) upon reasonable request. Please allow 3 weeks for a response.

Declarations

Ethics approval and consent to participate
The design of the present project was approved by the Institute Research Medical Ethics Committee of the Army Medical University (Approval number: 2020 No. 011–1) and the Ethics Committee at Kunming Institute of Zoology, Chinese Academy of Sciences (Approval number: KIZRKX-2021–010). All animal procedures were conducted in accordance with the guidelines approved by the Ethics Committee of the Kunming Institute of Zoology (approval number: IACUC-RE-2023–05-010). A written informed consent was obtained from each participant.

Consent for publication
Not applicable.

Competing interests
The authors declare that they have no competing interests.

Received: 30 January 2024 Accepted: 20 August 2024
Published online: 28 August 2024

References

1. Zhao F, Yang L, Zhang T, Zhuang D, Wu Q, Yu J, Tian C, Zhang Z. Gut microbiome signatures of extreme environment adaption in Tibetan pig. Npj Biofilms Microbi. 2023;9:27.
2. Zhao H, Sun L, Liu J, Shi B, Zhang Y, Qu-Zong CR, Dorji T, Wang T, Yuan H, Yang J. Meta-analysis identifying gut microbial biomarkers of Qinghai-Tibet Plateau populations and the functionality of microbiota-derived butyrate in high-altitude adaptation. Gut Microbes. 2024;16:2350151.
3. Turnbaugh PJ, Ley RE, Mahowald MA, Magrini V, Mardis ER, Gordon JI. An obesity-associated gut microbiome with increased capacity for energy harvest. Nature. 2006;444:1027–31.
4. Turnbaugh PJ, Hamady M, Yatsunenko T, Cantarel BL, Duncan A, Ley RE, Sogin ML, Jones WJ, Roe BA, Affourtit JP, et al. A core gut microbiome in obese and lean twins. Nature. 2009;457:480–4.
5. Li L, Zhao X. Comparative analyses of fecal microbiota in Tibetan and Chinese Han living at low or high altitude by barcoded 454 pyrosequencing. Sci Rep-Uk. 2015;5:14682.
6. Lan D, Ji W, Lin B, Chen Y, Huang C, Xiong X, Fu M, Mipam TD, Ai Y, Zeng B, et al. Correlations between gut microbiota community structures of Tibetans and geography. Sci Rep-Uk. 2017;7:16982.
7. Jia Z, Zhao X, Liu X, Zhao L, Jia Q, Shi J, Xu X, Hao L, Xu Z, Zhong Q, et al. Impacts of the plateau environment on the gut microbiota and blood clinical indexes in Han and Tibetan individuals. Msystems. 2020;5:e619–60.
8. Liu K, Zhang Y, Li Q, Li H, Long D, Yan S, Huang W, Long R, Huang X. Ethnic differences shape the alpha but not beta diversity of gut microbiota from school children in the absence of environmental differences. Microorganisms. 2020;8:254.
9. Zeng B, Zhang S, Xu H, Kong F, Yu X, Wang P, Yang M, Li D, Zhang M, Ni Q, et al. Gut microbiota of Tibetans and Tibetan pigs varies between high and low altitude environments. Microbiol Res. 2020;235:126447.
10. Cotillard A, Kennedy SP, Kong LC, Prifti E, Pons N, Le Chatelier E, Almeida M, Quinquis B, Levenez F, Galleron N, et al. Dietary intervention impact on gut microbial gene richness. Nature. 2013;500:585–8.
11. Kurilshikov A, Medina-Gomez C, Bacigalupe R, Radjabzadeh D, Wang J, Demirkan A, Le Roy CI, Raygoza GJ, Finnicum CT, Liu X, et al. Large-scale association analyses identify host factors influencing human gut microbiome composition. Nat Genet. 2021;53:156–65.
12. Rothschild D, Weissbrod O, Barkan E, Kurilshikov A, Korem T, Zeevi D, Costea PI, Godneva A, Kalka IN, Bar N, et al. Environment dominates over host genetics in shaping human gut microbiota. Nature. 2018;555:210–5.
13. Jain C, Rodriguez-R LM, Phillippy AM, Konstantinidis KT, Aluru S. High throughput ANI analysis of 90K prokaryotic genomes reveals clear species boundaries. Nat Commun. 2018;9:5114.
14. Pasolli E, Asnicar F, Manara S, Zolfo M, Karcher N, Armanini F, Beghini F, Manghi P, Tett A, Ghensi P, et al. Extensive unexplored human microbiome diversity revealed by over 150,000 genomes from metagenomes spanning age, geography, and lifestyle. Cell. 2019;176:649–62.
15. Schloissnig S, Arumugam M, Sunagawa S, Mitreva M, Tap J, Zhu A, Waller A, Mende DR, Kultima JR, Martin J, et al. Genomic variation landscape of the human gut microbiome. Nature. 2013;493:45–50.
16. Yu G, Gail MH, Consonni D, Carugno M, Humphrys M, Pesatori AC, Caporaso NE, Goedert JJ, Ravel J, Landi MT. Characterizing human lung tissue microbiota and its relationship to epidemiological and clinical features. Genome Biol. 2016;17:163.
17. Tian L, Wang X, Wu A, Fan Y, Friedman J, Dahlin A, Waldor MK, Weinstock GM, Weiss ST, Liu Y. Deciphering functional redundancy in the human microbiome. Nat Commun. 2020;11:6217.
18. Louca S, Polz MF, Mazel F, Albright M, Huber JA, O'Connor MI, Ackermann M, Hahn AS, Srivastava DS, Crowe SA, et al. Function and functional redundancy in microbial systems. Nat Ecol Evol. 2018;2:936–43.
19. Li Y, Ge Y, Wang J, Shen C, Wang J, Liu YJ. Functional redundancy and specific taxa modulate the contribution of prokaryotic diversity and composition to multifunctionality. Mol Ecol. 2021;30:2915–30.
20. Kang S, Ma W, Li FY, Zhang Q, Niu J, Ding Y, Han F, Sun X. Functional redundancy instead of species redundancy determines community stability in a typical steppe of inner Mongolia. PLoS ONE. 2015;10:e145605.
21. Lindenmayer DB, Margules CR. Botkin: Indicators of biodiversity for ecologically sustainable forest management. Conserv Biol. 2000;14:941–50.
22. Littlejohn PT, Metcalfe-Roach A, Cardenas Poire E, Holani R, Bar-Yoseph H, Fan YM, Woodward SE, Finlay BB. Multiple micronutrient deficiencies in early life cause multi-kingdom alterations in the gut microbiome and intrinsic antibiotic resistance genes in mice. Nat Microbiol. 2023;8:2392–405.
23. Roberts DW. labdsv: Ordination and multivariate analysis for ecology. R package version 2.0-1. The Comprehensive R Archive Network; 2013. https://cran.r-project.org/web/packages/labdsv/index.html. Accessed 1 Nov 2014.
24. Keshavarzian A, Green SJ, Engen PA, Voigt RM, Naqib A, Forsyth CB, Mutlu E, Shannon KM. Colonic bacterial composition in Parkinson's disease. Movement Disord. 2015;30:1351–60.
25. Liu X, Mao B, Gu J, Wu J, Cui S, Wang G, Zhao J, Zhang H, Chen W. Blautia-a new functional genus with potential probiotic properties? Gut Microbes. 2021;13:1–21.
26. Wang Y, Shi Y, Li W, Wang S, Zheng J, Xu G, Li G, Shen X, Yang J. Gut microbiota imbalance mediates intestinal barrier damage in high-altitude exposed mice. Febs J. 2022;289:4850–68.
27. Chelakkot C, Ghim J, Ryu SH. Mechanisms regulating intestinal barrier integrity and its pathological implications. Exp Mol Med. 2018;50:1–9.
28. Hosomi K, Saito M, Park J, Murakami H, Shibata N, Ando M, Nagatake T, Konishi K, Ohno H, Tanisawa K, et al. Oral administration of Blautia wexlerae ameliorates obesity and type 2 diabetes via metabolic remodeling of the gut microbiota. Nat Commun. 2022;13:4477.

29. Oksanen J, Blanchet FG, Kindt R, Legendre P, Minchin P, O'Hara B, Simpson G, Solymos P, Stevens H, Wagner H: Vegan: community ecology package. R Package Version 2.2–1. 2015;2:1–2.
30. Zhenda S, Qinghui K, Jiakui L, Suozhu L, Zhankun T, Peng S, Honghui W. Characterization of Bacterial microbial diversity in wild yak and domestic yak in Qiangtang Region of Tibet. Pak J Zool. 2015;54:1001–9.
31. Xu Y, Xiang S, Ye K, Zheng Y, Feng X, Zhu X, Chen J, Chen Y. Cobalamin (vitamin b12) induced a shift in microbial composition and metabolic activity in an in vitro colon simulation. Front Microbiol. 2018;9:2780.
32. Roth W, Mohamadzadeh M. Vitamin B12 and gut-brain homeostasis in the pathophysiology of ischemic stroke. EBioMedicine. 2021;73:103676.
33. Belzer C, Chia LW, Aalvink S, Chamlagain B, Piironen V, Knol J, de Vos WM. Microbial metabolic networks at the mucus layer lead to diet-independent butyrate and vitamin b(12) production by intestinal symbionts. MBio. 2017;8:e717–70.
34. Verstraeten S, Sencio V, Raise A, Huillet E, Layec S, Deruyter L, Heumel S, Auger S, Robert V, Langella P, et al. Description of a newly isolated blautia faecis strain and its benefit in mouse models of post-influenza secondary enteric and pulmonary infections. Nutrients. 2022;14:1478.
35. Abdugheni R, Wang WZ, Wang Y, Du MX, Liu FL, Zhou N, Jiang C, Wang CY, Wu L, Ma J, et al. Metabolite profiling of human-originated Lachnospiraceae at the strain level. Imeta. 2022;1:4.
36. Li A, Wang Y, Li Z, Qamar H, Mehmood K, Zhang L, Liu J, Zhang H, Li J. Probiotics isolated from yaks improves the growth performance, antioxidant activity, and cytokines related to immunity and inflammation in mice. Microb Cell Fact. 2019;18:112.
37. Wan Z, Zhang X, Jia X, Qin Y, Sun N, Xin J, Zeng Y, Jing B, Fang J, Pan K, et al. Lactobacillus johnsonii YH1136 plays a protective role against endogenous pathogenic bacteria induced intestinal dysfunction by reconstructing gut microbiota in mice exposed at high altitude. Front Immunol. 2022;13:1007737.
38. Dou X, Zhang B, Qiao L, Song X, Pi S, Chang J, Zhang X, Zeng X, Zhu L, Xu C. Biogenic selenium nanoparticles synthesized by Lactobacillus casei ATCC 393 alleviate acute hypobaric hypoxia-induced intestinal barrier dysfunction in C57BL/6 mice. Biol Trace Elem Res. 2023;201:4484–96.
39. Zhang X, Jia X, Wang S, Xin J, Sun N, Wang Y, Zhang X, Wan Z, Fan J, Li H, et al. Disrupted gut microbiota aggravates spatial memory dysfunction induced by high altitude exposure: a link between plateau environment and microbiome-gut-brain axis. Ecotox Environ Safe. 2023;259:115035.
40. Morgavi DP, Forano E, Martin C, Newbold CJ. Microbial ecosystem and methanogenesis in ruminants. Animal. 2010;4:1024–36.
41. Ma Y, Ma S, Chang L, Wang H, Ga Q, Ma L, Bai Z, Shen Y, Ge RL. Gut microbiota adaptation to high altitude in indigenous animals. Biochem Bioph Res Co. 2019;516:120–6.
42. Liu H, Han X, Zhao N, Hu L, Wang X, Luo C, Chen Y, Zhao X, Xu S. The gut microbiota determines the high-altitude adaptability of Tibetan wild asses (Equus kiang) in Qinghai-Tibet Plateau. Front Microbiol. 2022;13:949002.
43. Smith PM, Howitt MR, Panikov N, Michaud M, Gallini CA, Bohlooly-Y M, Glickman JN, Garrett WS. The microbial metabolites, short-chain fatty acids, regulate colonic Treg cell homeostasis. Science. 2013;341:569–73.
44. Chen S, Zhou Y, Chen Y, Jia G. fastp: an ultra-fast all-in-one FASTQ preprocessor. Bioinformatics. 2018;34:i884–90.
45. Langmead B, Salzberg SL. Fast gapped-read alignment with Bowtie 2. Nat Methods. 2012;9:357–9.
46. Li D, Liu CM, Luo R, Kunihiko S, Tak-Wah L. MEGAHIT: an ultra-fast single-node solution for large and complex metagenomics assembly via succinct de Bruijn graph. Bioinformatics. 2015;31:1674–6.
47. Uritskiy GV, DiRuggiero J, Taylor J. MetaWRAP-a flexible pipeline for genome-resolved metagenomic data analysis. Microbiome. 2018;6:158.
48. Parks DH, Imelfort M, Skennerton CT, Hugenholtz P, Tyson GW. CheckM: assessing the quality of microbial genomes recovered from isolates, single cells, and metagenomes. Genome Res. 2015;25:1043–55.
49. Olm MR, Brown CT, Brooks B, Banfield JF. dRep: a tool for fast and accurate genomic comparisons that enables improved genome recovery from metagenomes through de-replication. Isme J. 2017;11:2864–8.
50. Chaumeil PA, Mussig AJ, Hugenholtz P, Parks DH. GTDB-Tk: a toolkit to classify genomes with the Genome Taxonomy Database. Bioinformatics. 2019;36:1925–7.
51. Asnicar F, Weingart G, Tickle TL, Huttenhower C, Segata N. Compact graphical representation of phylogenetic data and metadata with GraPhlAn. PeerJ. 2015;3:e1029.
52. Huson DH, Buchfink B. Fast and sensitive protein alignment using DIAMOND. Nat Methods. 2015;12:59–60.
53. Peng X, Wilken SE, Lankiewicz TS, Gilmore SP, Brown JL, Henske JK, Swift CL, Salamov A, Barry K, Grigoriev IV, et al. Genomic and functional analyses of fungal and bacterial consortia that enable lignocellulose breakdown in goat gut microbiomes. Nat Microbiol. 2021;6:499–511.
54. Boix E, Coroller L, Couvert O, Planchon S, van Vliet AHM, Brunt J, Peck MW, Rasetti-Escargueil C, Lemichez E, Popoff MR, et al. Synergistic interaction between pH and NaCl in the limits of germination and outgrowth of Clostridium sporogenes and Group I Clostridium botulinum vegetative cells and spores after heat treatment. Food Microbiol. 2022;106:104055.
55. Thibault HB, Kurtz B, Raher MJ, Shaik RS, Waxman A, Derumeaux G, Halpern EF, Bloch KD, Scherrer-Crosbie M. Noninvasive assessment of murine pulmonary arterial pressure: validation and application to models of pulmonary hypertension. Circ-Cardiovasc Imag. 2010;3:157–63.
56. Champion HC, Michelakis ED, Hassoun PM. Comprehensive invasive and noninvasive approach to the right ventricle-pulmonary circulation unit: state of the art and clinical and research implications. Circulation. 2009;120:992–1007.
57. Nagaishi T, Watabe T, Kotake K, Kumazawa T, Aida T, Tanaka K, Ono R, Ishino F, Usami T, Miura T, et al. Immunoglobulin A-specific deficiency induces spontaneous inflammation specifically in the ileum. Gut. 2022;71:487–96.
58. Zhang Q, Zhao Q, Li T, Lu L, Wang F, Zhang H, Liu Z, Ma H, Zhu Q, Wang J, et al. Lactobacillus plantarum-derived indole-3-lactic acid ameliorates colorectal tumorigenesis via epigenetic regulation of CD8(+) T cell immunity. Cell Metab. 2023;35:943–60.

59. Chen S, Chen L, Qi Y, Xu J, Ge Q, Fan Y, Chen D, Zhang Y, Wang L, Hou T, et al. Bifidobacterium adolescentis regulates catalase activity and host metabolism and improves healthspan and lifespan in multiple species. Nat Aging. 2021;1:991–1001.
60. Blanco-Míguez A, Beghini F, Cumbo F, McIver LJ, Thompson KN, Zolfo M, Manghi P, Dubois L, Huang KD, Thomas AM, et al. Extending and improving metagenomic taxonomic profiling with uncharacterized species using MetaPhlAn 4. Nat Biotechnol. 2023;41:1633–44.
61. Rohart F, Gautier B, Singh A, Lê CK. mixOmics: an R package for 'omics feature selection and multiple data integration. Plos Comput Biol. 2017;13:e1005752.
62. Zhang J, Guo Z, Xue Z, Sun Z, Zhang M, Wang L, Wang G, Wang F, Xu J, Cao H, et al. A phylo-functional core of gut microbiota in healthy young Chinese cohorts across lifestyles, geography and ethnicities. Isme J. 2015;9:1979–90.
63. Chen T, Chen X, Zhang S, Zhu J, Tang B, Wang A, Dong L, Zhang Z, Yu C, Sun Y, et al. The genome sequence archive family: toward explosive data growth and diverse data types. Genomics Proteomics Bioinformatics. 2021;19:578–83.
64. Database Resources of the National Genomics Data Center. China National Center for Bioinformation in 2024. Nucleic Acids Res. 2024;52:D18–32.
65. Su Q, Zhuang DH , Li YC, Chen Y, Wang XY, Ge MX, Xue TY, Zhang QY, Liu XY, Yin FQ, Han YM, Gao ZL, Zhao L, Li YX, Lv MJ, Yang LQ, Xia TR,Luo YJ, Zhang ZG, Kong QP. Study on the gut microbiota of 46 han nationality in plain areas exposed to high altitude hypoxia. Datasets. Genome Sequence Archive-human; 2024. https://bigd.big.ac.cn/gsa-human/browse/HRA003616. Accessed 31 Jul 2024.
66. Su Q, Zhuang DH , Li YC, Chen Y, Wang XY, Ge MX, Xue TY, Zhang QY, Liu XY, Yin FQ, Han YM, Gao ZL, Zhao L, Li YX, Lv MJ, Yang LQ, Xia TR,Luo YJ, Zhang ZG, Kong QP. Metagenomic data of mice exposed to hypoxia. Datasets. Genome Sequence Archive; 2024. https://ngdc.cncb.ac.cn/gsa. Accessed 1 Aug 2024.
67. Pasolli E, Asnicar F, Manara S, Zolfo M, Karcher N, Armanini F, Beghini F, Manghi P, Tett A, Ghensi P, Collado MC, Rice BL, DuLong C, Morgan XC, Golden CD, Quince C, Huttenhower C, Segata N. The 4,930 SGBs' representatives. Datasets. University of Trento; 2019. http://segatalab.cibio.unitn.it/data/Pasolli_et_al.html. Accessed 24 Jan 2019.
68. Kong QP, Su Q, Li YC, Wang XY. Raw data from histological sections of hypoxic exposed mice. Zenodo; 2024. https://zenodo.org/records/13147420

Publisher's Note